REPORT

ELECTROCHEMISTRY

CO_2 electrolysis to multicarbon products in strong acid

Jianan Erick Huang[1]†, Fengwang Li[1,2]*†, Adnan Ozden[3]†, Armin Sedighian Rasouli[1], F. Pelayo García de Arquer[1]‡, Shijie Liu[3], Shuzhen Zhang[2], Mingchuan Luo[1], Xue Wang[1], Yanwei Lum[1], Yi Xu[3], Koen Bertens[1], Rui Kai Miao[3], Cao-Thang Dinh[1], David Sinton[3]*, Edward H. Sargent[1]*

Carbon dioxide electroreduction (CO_2R) is being actively studied as a promising route to convert carbon emissions to valuable chemicals and fuels. However, the fraction of input CO_2 that is productively reduced has typically been very low, <2% for multicarbon products; the balance reacts with hydroxide to form carbonate in both alkaline and neutral reactors. Acidic electrolytes would overcome this limitation, but hydrogen evolution has hitherto dominated under those conditions. We report that concentrating potassium cations in the vicinity of electrochemically active sites accelerates CO_2 activation to enable efficient CO_2R in acid. We achieve CO_2R on copper at pH <1 with a single-pass CO_2 utilization of 77%, including a conversion efficiency of 50% toward multicarbon products (ethylene, ethanol, and 1-propanol) at a current density of 1.2 amperes per square centimeter and a full-cell voltage of 4.2 volts.

Electrochemical reduction of CO_2 (CO_2R) using renewable electricity offers an attractive approach to produce widely needed chemicals and feedstocks while mitigating greenhouse gas emissions (*1*, *2*). Effort has been dedicated to developing catalysts that achieve high faradaic efficiency (FE) toward carbon monoxide and formate and to promoting C–C coupling toward multicarbon (C_{2+}) products such as ethylene and ethanol (*3*–*6*). Lowering overpotentials of these reactions and increasing their productivity (current density) have been priorities for the field (*7*, *8*).

Despite many recent advances, CO_2R remains far from practical viability because strong local alkaline conditions are present (Fig. 1A). Rather than being reduced, a major fraction of the input CO_2 is instead consumed in the electrolyte through reaction with OH^- to produce CO_3^{2-}

$$2OH^-_{(aq)} + CO_{2\,(g)} \rightarrow CO_3^{2-}{}_{(aq)} + H_2O_{(l)}$$

Carbonate formation imposes a limit of carbon utilization efficiency (fraction of CO_2 in the input feed converted to CO_2R products) that is prohibitively low (*9*). For every H_2O-electron pair transferred during CO_2R, one hydroxide is produced at the cathode, reacting with ½ CO_2 to form carbonate. As a result, the maximum carbon efficiency is 50% for two-electron-transfer processes such as CO_2 to CO.

For CO_2R to more valuable C_{2+} products, the effect is even more acute: The carbon efficiency of CO_2R to ethylene or ethanol is limited to 25%, as six electrons are needed per CO_2 reacted. In practice, due in part to nonunity selectivity and use of alkaline electrolyte, the carbon efficiency is even lower than these best-case theoretical limits (Fig. 1B) (*7*, *10*–*15*).

Dealing with CO_2 loss in alkaline and neutral environments leads to a severe energy penalty if one seeks to recycle the emitter CO_2 from carbonate or cathodic and anodic streams (*16*). Technoeconomic analysis of alkaline CO_2 electrolyzers shows that >50% of input energy is used to regenerate CO_2 lost to carbonate (Fig. 1C and tables S1 and S2; details in supplementary materials). CO_2 electrolyzers using neutral electrolyte produce a local alkaline environment under operating conditions and thus also suffer from carbonate formation and crossover (*17*, *18*). The problem of inefficient CO_2 utilization in CO_2R is central to the field and severely limits its prospects (*9*). While advances in FE and current density have been steady, the utilization challenge demands a new approach.

CO_2R in acidic media offers an avenue to reduce carbonate formation to near zero and thus also eliminate CO_2 crossover (Fig. 1, D and E). Specifically, when H_3O^+ is the proton source for CO_2R, no OH^- is generated, and CO_2 conversion can proceed without carbonate formation; when H_2O is the proton source, any carbonate generated locally will lie within the diffusion layer and be converted back to CO_2 by protons in the bulk electrolyte (*19*). Initial tests using phosphate buffer electrolytes (pH 1 to 4; see supplementary materials for detailed preparation methods) showed no measurable loss of CO_2 to the anode at 400 mA/cm^2 over 6 hours compared with a loss of ~70% of input CO_2 in the reference case with bicarbonate electrolyte (Fig. 1F and fig. S1). However, under acidic conditions, the kinetically more favorable hydrogen evolution reaction (HER) outcompetes the reduction of CO_2, with CO_2R FE close to zero in strong acids (pH <1). These results are in agreement with past work on acidic CO_2R, in which only single-carbon products, such as CO and methane, were observed in electrolytes of elevated pH in the range 3 to 5 (*19*–*25*); one of these works achieved near 100% FE to CO in pH 3 electrolyte (*19*).

In this study, we pursued a cation augmenting strategy to improve CO_2 activation kinetics in strong acid (pH <1). We used high-concentration phosphate buffer (total phosphorus species kept to 1 M) as electrolyte to keep pH locally at the cathode as close as possible to that at the bulk (*26*). Modeling of reaction and diffusion of species within a typical diffusion layer of 50 μm indicates that, in the phosphoric acid (H_3PO_4, 1 M, pH 1.05) electrolyte, the surface (distance to cathode of 0 μm) pH is similar to the bulk at current densities <200 mA/cm^2 while becoming neutral and alkaline when current densities increase further (Fig. 2A, fig. S2, and tables S3 to S5; details in supplementary materials). The locally alkaline conditions result from a consumption rate of local protons that exceeds mass transport of protons from the bulk (*27*). Despite elevated pH at the surface, pH decreases to an acidic range within a short distance of the cathode. Even at a current density as high as 1 A/cm^2, the pH decreases to 6.3 [first acid dissociation constant (pK_{a1}) of carbonic acid] within 33 μm of the electrode. This confinement assures that any locally generated carbonate would be converted back to CO_2 for ensuing reduction, avoiding carbonate crossover and the associated loss of reactant CO_2. In comparison, similar conditions (pH 6.3 at a distance to cathode of 30 μm) are reached at much lower current densities (<200 mA/cm^2) in electrolytes of pH 2 to 4 (fig. S2). In the interest of realizing economic CO_2 electrolyzers (*28*), we focus this study on high-rate CO_2 electrolysis in strong acid (pH ≤1).

To circumvent the kinetically more favorable HER in acid, we sought to operate CO_2R at current densities where the H_3O^+ mass-transport limitation occurs and H_2O becomes the main proton donor at the cathode surface (*19*, *22*). Modeling shows that the surface pH

[1]Department of Electrical and Computer Engineering, University of Toronto, Toronto, ON M5S 1A4, Canada. [2]School of Chemical and Biomolecular Engineering and University of Sydney Nano Institute, University of Sydney, Sydney, NSW 2006, Australia. [3]Department of Mechanical and Industrial Engineering, University of Toronto, Toronto, ON M5S 3G8, Canada.
*Corresponding author. Email: ted.sargent@utoronto.ca (E.H.S.); sinton@mie.utoronto.ca (D.S.); fengwang.li@sydney.edu.au (F.L.)
†These authors contributed equally to this work.
‡Present address: ICFO – Institut de Ciències Fotòniques, Barcelona Institute of Science and Technology, Barcelona 08860, Spain.

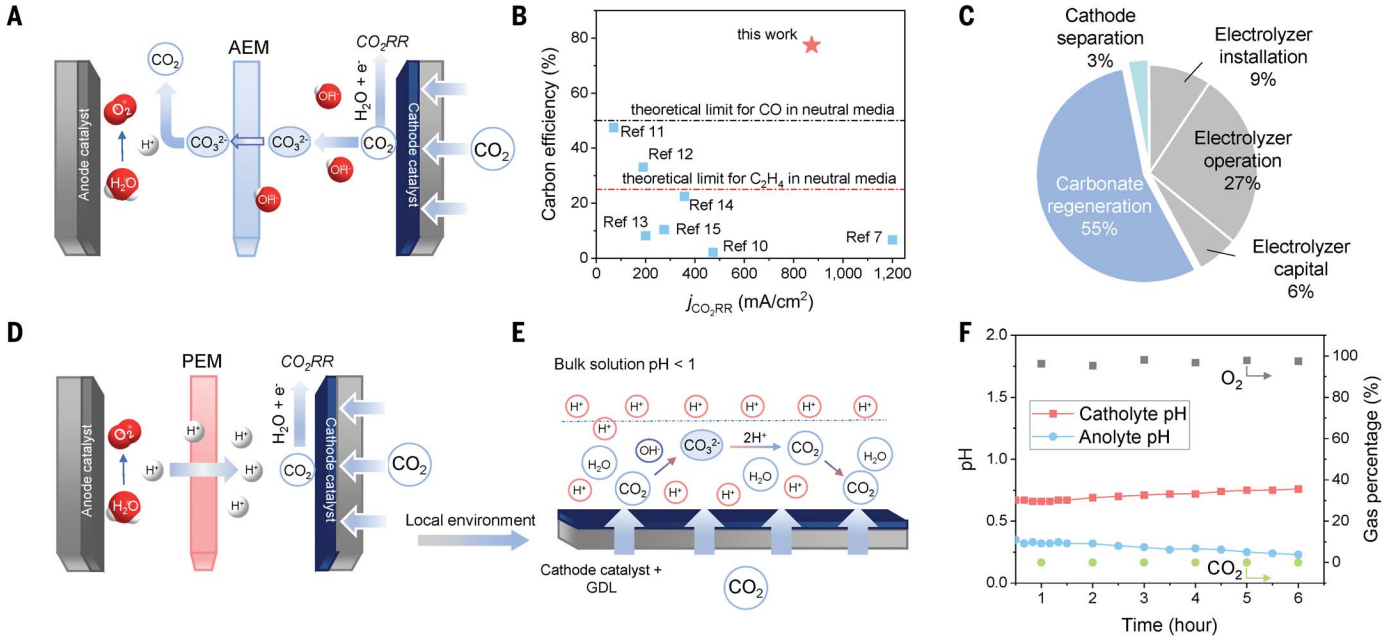

Fig. 1. Acidic CO_2 reduction versus alkaline and neutral CO_2 reduction. (**A**) Schematic of carbonate formation and crossover phenomenon observed in neutral electrolyte–based reactor using anion exchange membrane (AEM). CO_2RR, CO_2 reduction reaction. (**B**) Comparison of carbon efficiency and current density in the benchmark alkaline and neutral CO_2R electrolyzers (*7*, *10*–*15*). The dashed lines indicate theoretical carbon efficiency for CO (black) and C_2H_4 (red), respectively, in neutral media. Carbon efficiency in alkaline media is lower than in neutral media owing to additional consumption of CO_2 by bulk OH^-. (**C**) Cost breakdown of an alkaline CO_2R flow cell based on technoeconomic analysis (see supplementary materials for details; see also tables S1 and S2). (**D** and **E**) Schematics of ion transport and reactions in acidic CO_2R reactors. PEM, proton exchange membrane; GDL, gas diffusion layer. (**F**) Product analysis of the outlet gases at the anode side and monitoring of pH of catholyte and anolyte in a flow cell comprising 1 M H_3PO_4 and 3 M KCl as the catholyte, 0.5 M H_2SO_4 as the anolyte, and Nafion as the membrane. The cell was operated at a constant current density of 400 mA/cm^2.

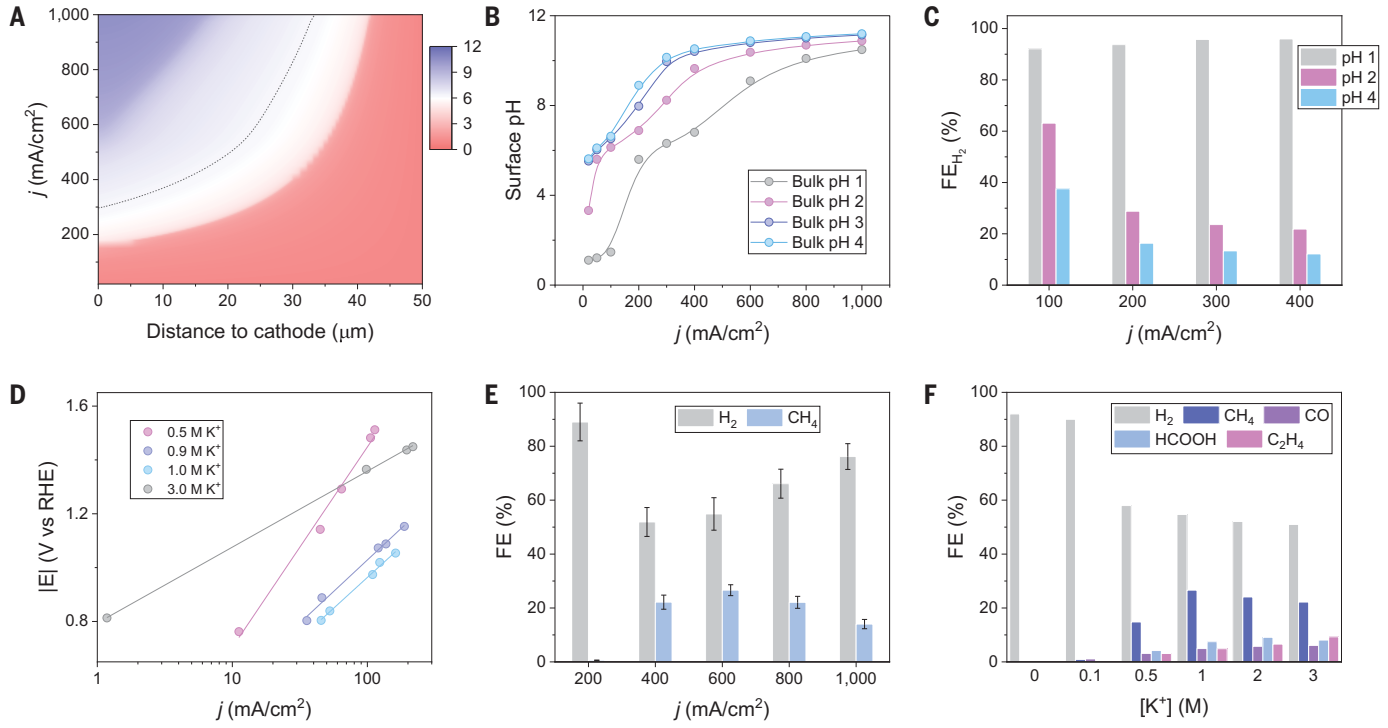

Fig. 2. Cation-enabled CO_2 reduction in acidic electrolyte. (**A**) Modeling of pH at different distances to cathode and current density in 1 M H_3PO_4 and 3 M KCl. The pH was adjusted to 1 by KOH. See supplementary materials for modeling details. (**B**) Surface (distance to cathode of 0 μm) pH at various pH and current density values. (**C**) FE toward hydrogen at current densities from 100 to 400 mA/cm^2 in phosphate electrolytes with different pH values. (**D**) Tafel slopes obtained in electrolyte with different K^+ concentrations. (**E**) FE toward H_2 and CH_4 on sputtered Cu catalyst at different current densities in 1 M H_3PO_4 and 3 M KCl. Values are means, and error bars indicate SD (n = 3 replicates). (**F**) FE toward all products on sputtered Cu catalyst in 1 M H_3PO_4 with different KCl concentrations at 400 mA/cm^2.

approaches neutrality when the current density reaches 100 mA/cm^2 for electrolytes with pH 2 to 4, or above 200 mA/cm^2 for electrolyte with pH 1 (Fig. 2B). Indeed, we observed experimentally a marked decrease of HER selectivity in electrolytes with pH 2 and 4 at a current density range of 100 to 400 mA/cm^2; however, no measurable CO_2R products were detected in electrolyte with pH 1, even at a current density of 400 mA/cm^2 (Fig. 2C and fig. S3), at which the surface pH was modeled to be 7.

When we added 0.5 M KCl into the H_3PO_4 electrolyte (pH 1) in the middle of the reaction, however, we observed a slight decrease in FE toward hydrogen and detected CH_4 (FE 2.1 ± 0.3%) at a current density of 200 mA/cm^2 (fig. S4). Noting that the phosphate buffer electrolytes with different pH were prepared by mixing H_3PO_4 and KH_2PO_4 at different ratios, we posited that ion species, particularly cations (*29*–*31*), might steer kinetics of CO_2R catalysis at bulk pH <1.

To test this hypothesis, we carried out Tafel analysis at different pH and found that the Tafel slope decreased along with an increase in K^+ concentration in the electrolytes (Fig. 2D). The slope reaches a minimum of 0.28 volts per decade at an electrolyte composition of 1 M H_3PO_4 with 3 M KCl (pH 0.67). This result suggests that the change in Tafel slope is not attributable to pH and that the rate-determining step is the adsorption of CO_2 (*25*). The presence of cations is key to CO_2 activation on the catalyst surface. Previous studies attributed the enhanced activation achieved with cations to their electrostatic interactions with the electric dipole of adsorbates or changes of surface charge density (*30*, *31*). We assessed this activation enhancement on silver catalysts; in 1 M H_3PO_4 electrolyte, no CO_2R reactivity was observed, whereas ~50% CO_2R selectivity was achieved in the presence of 3 M K^+ in the same electrolyte (fig. S5). The CO_2R selectivity on Cu catalysts was dependent on current density, and the FE of the main CO_2R product, CH_4, reached a maximum of 27% at 600 mA/cm^2 (Fig. 2E).

We studied the impact of local pH (equivalent to concentration of protons accessible to CO_2R and HER) on the activation of CO_2 and suppression of HER. At current densities <200 mA/cm^2, in which the local pH in 1 M H_3PO_4 electrolyte exhibits pH ≪7, the addition of K^+ into the electrolyte did not affect voltametric properties of the Cu electrode, regardless of the concentration of K^+ and the atmosphere (N_2 versus CO_2) (fig. S6), suggesting that K^+ does not play a role in the activation of CO_2 nor does it suppress HER (from proton reduction) in a locally acidic environment. However, when operating at a higher current density of 400 mA/cm^2 to deplete local protons (local pH >7), while adding K^+ did not affect applied potentials, it did tune selectivity from HER (from water reduction) to CO_2R. The change of gas flow from N_2 to CO_2 increased the CO_2R partial current density from 0 to nearly 200 mA/cm^2 and decreased HER partial current density by about the same amount, but we did not observe any CO_2R activity in the electrolyte without K^+ (fig. S7). These observations indicate a full mechanistic picture for CO_2R in bulk acidic electrolyte: Under a proton-depletion local environment, the cation triggers CO_2 activation, which suppresses the HER from water reduction, consistent with prior reports (*19*, *32*).

The effect of anions on CO_2R reactivity is not significant; substitution of SO_4^{2-} or I^- for Cl^- showed product distribution similar to that of the Cl^- case (fig. S8). It is unlikely that K^+ affects the oxidation state of Cu catalysts. Only metallic Cu was observed by operando x-ray absorption spectroscopy (fig. S9).

We examined CO_2R product distribution in 1 M H_3PO_4 with different concentrations of K^+, and current density remained constant at 400 mA/cm^2 (Fig. 2F). The HER selectivity decreased with an increase in K^+ concentration, and CO_2R selectivity increased. Selectivity for CH_4 was the highest, at ~28%, for 1 M K^+. The FE toward C_2H_4, although not dominant, increased steadily from 3.1% with 0.5 M K^+ to 9.3% with 3 M K^+.

We sought to selectively steer further toward C_2H_4, in light of its high value and broad application in chemical manufacturing (*33*). However, the solubility of K^+ in aqueous electrolytes is limited while maintaining a low pH. We turned to the enrichment of K^+ at the Cu surface by a cation-augmenting layer (CAL). We used a cationic perfluorosulfonic acid (PFSA) ionomer composed of tetrafluoroethylene and sulfonyl fluoride vinyl ether. The acidic $-SO_3H$ group is expected to exchange its protons with K^+ from the bulk electrolyte in a nonacidic local environment, sustaining a high K^+ concentration at the catalyst surface (Fig. 3A). In addition, the CAL allows cation (e.g., H^+ and K^+) transport in the direction from electrolyte to catalyst surface while slowing OH^- diffusion out, leading to higher surface pH, which was reported to facilitate C–C coupling (*10*, *15*, *34*). The ionomer was loaded onto the sputtered Cu surface as a blend with carbon nanoparticles (NPs) to increase its adhesion to the catalyst (fig. S10; details in supplementary materials).

The CAL-modified Cu showed a further increase of FE toward C_2H_4 to 13% and a much lower FE toward CH_4 of <1% compared with the bare Cu catalyst, while the remaining CO_2R gaseous product was CO at a current density of 400 mA/cm^2 in 1 M H_3PO_4 with 3 M KCl (Fig. 3B). The product selectivity shift was attributed to electrostatic interactions of cation species (e.g., K^+) with the electric dipole of specific adsorbates that favor C_{2+} reaction pathways (*31*, *35*). The FE toward C_2H_4 was ~10% for current densities in the range 300 to 800 mA/cm^2 (fig. S11). X-ray photoelectron spectroscopy (XPS) showed a marked increase of potassium on the CAL-modified Cu surface compared with the bare Cu after CO_2R operation (fig. S12), confirming the preservation of K^+ by the ionomer layer.

To improve CO_2R productivity still further, we increased the electrochemically active surface area of the electrode by forming a Cu-NPs/PFSA composite material (fig. S13; details in supplementary materials) (*7*, *36*). Similar to the case of bare Cu, the CO_2R selectivity was dependent on the bulk concentration of K^+ in 1 M H_3PO_4; the FE toward C_2H_4 increased from ~10% with 1 M K^+ to 26% with 3 M K^+ at a current density of 1.2 A/cm^2 (Fig. 3C and fig. S14). The overall CO_2R selectivity reached 61%, including a total C_{2+} FE of 40%.

Using a slim, low-resistance flow cell (fig. S15), we operated the high-surface-area CAL-modified Cu electrode at a current density of 1.2 A/cm^2 stably for an initial 12-hour test (details in supplementary materials). The full-cell voltage was 4.2 V (without compensation of voltage drop due to solution resistance, *i*R) and the FE toward C_2H_4 was constantly ~25% (Fig. 3D and fig. S16). In-depth XPS analyses indicate that K distributed evenly across the top layer of the composite electrode after CO_2R reaction (fig. S17). The percentages of Cl and P were five times lower than that of K, suggesting that the observed K concentration was sustained by the ionomer rather than caused by residual electrolyte salts.

CO_2R in acid enables CO_2 electrolysis without carbonate formation and crossover in bulk electrolytes, circumventing the CO_2 utilization limit that is fundamental to neutral and alkaline systems and permitting a carbon efficiency that is capable of increasing further in the direction of unity. To reduce energy demand of product separation from dilute streams (*37*), we pursued single-pass carbon efficiency (SPCE) toward the new theoretical limit.

By gradually reducing the flow rate of CO_2 from 50 to 5 standard cubic centimeters per minute (sccm), the C_{2+} FE was improved to 48% (31% toward C_2H_4, 12% toward C_2H_5OH, 4% toward C_3H_7OH, and 1% toward CH_3COOH) (fig. S18). This combination of current density and selectivity results in a high overall C_{2+} productivity of 600 mA/cm^2 (Fig. 3E).

By further lowering the flow rate of CO_2 to 3 sccm, we achieved, at a current density of 1.2 A/cm^2, an SPCE of ~77% for all the CO_2R products, including ~50% for C_{2+} products (Fig. 3F). This outperforms previously reported alkaline and neutral CO_2R electrolyzers (Fig. 1B and table S6).

The cation augmentation takes CO_2 electrolysis from high-pH neutral and alkaline electrolytes to a pH <1 acidic environment. The

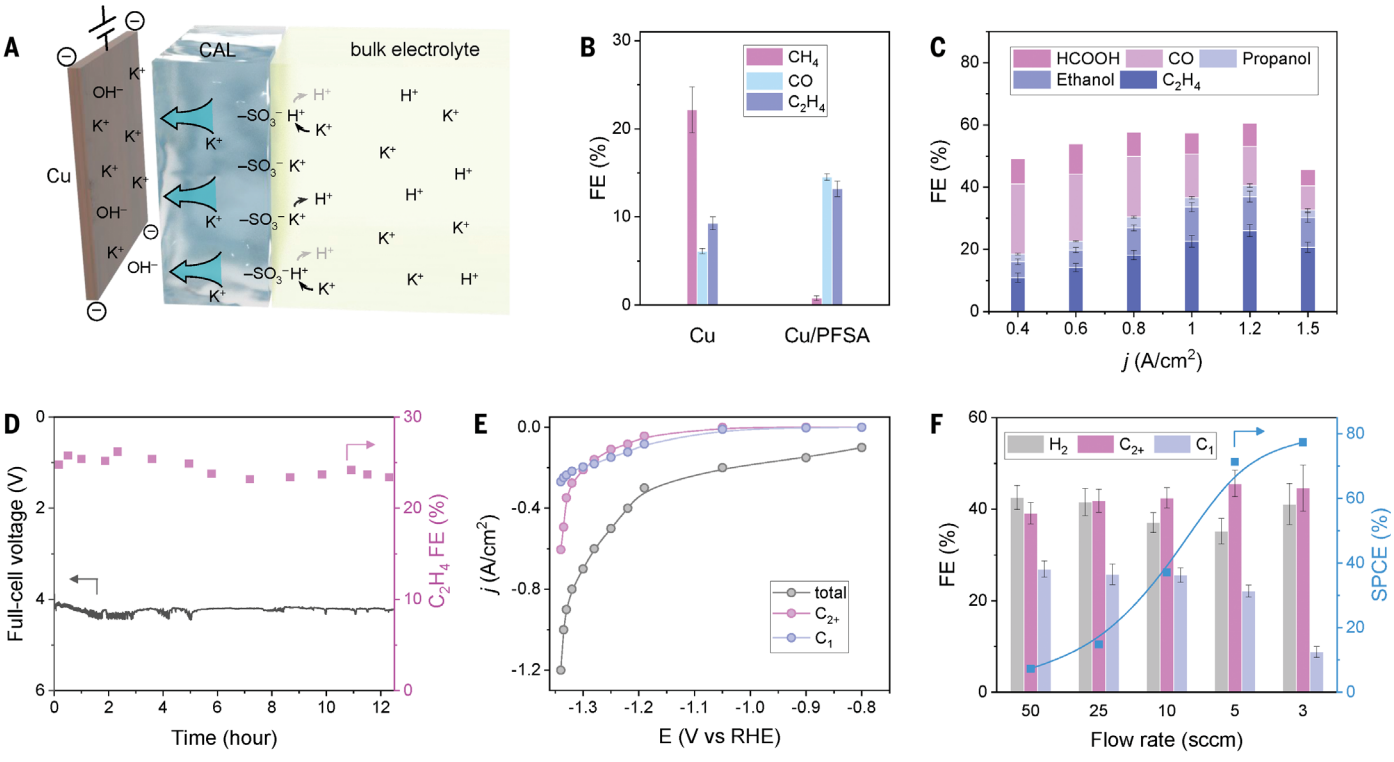

Fig. 3. Cation-augmenting layer (CAL) for multicarbon product formation and high carbon efficiency in acidic electrolyte. (**A**) Schematic illustration of ionic environment and transport near the catalyst surface functionalized by the PFSA ionomer. (**B**) FEs toward gaseous CO_2R products on bare Cu and PFSA-modified Cu (Cu/PFSA) at 400 mA/cm^{-2} in 1 M H_3PO_4 with 3 M KCl. Values are means, and error bars indicate SD (n = 3 replicates). (**C**) FEs toward CO_2R products at 400 to 1500 mA cm^{-2} on CAL-modified Cu electrode. The flow rate of CO_2 inlet was 50 sccm. Values are means, and error bars indicate SD (n = 3 replicates). (**D**) The extended CO_2R performance of the CAL-modified Cu-NP electrode in a slim flow cell at a constant current density of 1.2 A cm^{-2}. Nafion 117 membrane was used as the cation exchange membrane and high-surface-area IrO_x-Ti catalyst was used as the anode electrode. (**E**) Current density toward CO_2R products on CAL-modified Cu electrode. The flow rate of CO_2 inlet was 5 sccm. (**F**) FEs toward H_2 and CO_2R products as well as SPCE on CAL-modified Cu electrode at 1.2 A cm^{-2} with different CO_2 flow rates. All experiments were performed using 1 M H_3PO_4 + 3 M KCl catholyte. Values are means, and error bars indicate SD (n = 3 replicates).

approach overcomes the problems of carbonate formation and CO_2 crossover. A voltage breakdown analysis shows that the full-cell voltage required to operate in this acidic system is comparable to that in the state-of-art neutral membrane electrode assembly cells (fig. S19) (*7*). We note that further improvement in selectivity and a decrease in operating voltage will be required on the path to energy-efficient electrochemical CO_2 conversion.

REFERENCES AND NOTES

1. S. Chu, A. Majumdar, *Nature* **488**, 294–303 (2012).
2. P. De Luna *et al.*, *Science* **364**, eaav3506 (2019).
3. S. Ren *et al.*, *Science* **365**, 367–369 (2019).
4. Y. Wu, Z. Jiang, X. Lu, Y. Liang, H. Wang, *Nature* **575**, 639–642 (2019).
5. B. A. Rosen *et al.*, *Science* **334**, 643–644 (2011).
6. H. Xu *et al.*, *Nat. Energy* **5**, 623–632 (2020).
7. F. P. García de Arquer *et al.*, *Science* **367**, 661–666 (2020).
8. W. Ma *et al.*, *Nat. Catal.* **3**, 478–487 (2020).
9. J. A. Rabinowitz, M. W. Kanan, *Nat. Commun.* **11**, 5231 (2020).
10. C.-T. Dinh *et al.*, *Science* **360**, 783–787 (2018).
11. T. Haas, R. Krause, R. Weber, M. Demler, G. Schmid, *Nat. Catal.* **1**, 32–39 (2018).
12. R. B. Kutz *et al.*, *Energy Technol.* **5**, 929–936 (2017).
13. S. Verma *et al.*, *ACS Energy Lett.* **3**, 193–198 (2018).
14. T. T. H. Hoang *et al.*, *J. Am. Chem. Soc.* **140**, 5791–5797 (2018).
15. S. Ma *et al.*, *J. Power Sources* **301**, 219–228 (2016).
16. D. W. Keith, G. Holmes, D. St. Angelo, K. Heidel, *Joule* **2**, 1573–1594 (2018).
17. M. Ma *et al.*, *Energy Environ. Sci.* **13**, 977–985 (2020).
18. F. Li *et al.*, *Nature* **577**, 509–513 (2020).
19. C. J. Bondue, M. Graf, A. Goyal, M. T. M. Koper, *J. Am. Chem. Soc.* **143**, 279–285 (2021).
20. Z. Wang, P. Hou, Y. Wang, X. Xiang, P. Kang, *ACS Sustain. Chem. Eng.* **7**, 6106–6112 (2019).
21. R. Kortlever, C. Balemans, Y. Kwon, M. T. M. Koper, *Catal. Today* **244**, 58–62 (2015).
22. H. Ooka, M. C. Figueiredo, M. T. M. Koper, *Langmuir* **33**, 9307–9313 (2017).
23. Y. Liu, C. C. L. McCrory, *Nat. Commun.* **10**, 1683 (2019).
24. Y. Wu *et al.*, *Electrochemistry* **88**, 359–364 (2020).
25. J. Shen *et al.*, *Nat. Commun.* **6**, 8177 (2015).
26. I. Katsounaros *et al.*, *Electrochem. Commun.* **13**, 634–637 (2011).
27. N. Gupta, M. Gattrell, B. MacDougall, *J. Appl. Electrochem.* **36**, 161–172 (2006).
28. M. Jouny, W. W. Luc, F. Jiao, *Ind. Eng. Chem. Res.* **57**, 2165–2177 (2018).
29. A. Murata, Y. Hori, *Bull. Chem. Soc. Jpn.* **64**, 123–127 (1991).
30. S. Ringe *et al.*, *Energy Environ. Sci.* **12**, 3001–3014 (2019).
31. J. Resasco *et al.*, *J. Am. Chem. Soc.* **139**, 11277–11287 (2017).
32. S. Ringe *et al.*, *Nat. Commun.* **11**, 33 (2020).
33. H. Zimmermann, R. Walzl, in *Ullmann's Encyclopedia of Industrial Chemistry* (Wiley-VCH, 2009).
34. J. H. Montoya, C. Shi, K. Chan, J. K. Nørskov, *J. Phys. Chem. Lett.* **6**, 2032–2037 (2015).
35. R. B. Sandberg, J. H. Montoya, K. Chan, J. K. Nørskov, *Surf. Sci.* **654**, 56–62 (2016).
36. A. Ozden *et al.*, *ACS Energy Lett.* **5**, 2811–2818 (2020).
37. D. S. Ripatti, T. R. Veltman, M. W. Kanan, *Joule* **3**, 240–256 (2019).

ACKNOWLEDGMENTS

We thank T. Wu and G. Sterbinsky for technical support at 9BM beamline of Advanced Photon Source (APS). **Funding:** This work was financially supported by the Ontario Research Foundation: Research Excellence Program, the Natural Sciences and Engineering Research Council (NSERC) of Canada, TOTAL SE, and Australian Research Council (project number DE200100477). This research used synchrotron resources of the APS, an Office of Science User Facility operated for the U.S. Department of Energy (DOE) Office of Science by Argonne National Laboratory, and was supported by the U.S. DOE under contract no. DE-AC02-06CH11357, and the Canadian Light Source and its funding partners. **Author contributions:** E.H.S., F.L., and D.S. supervised the project. F.L. and C.-T.D. conceived of the idea. J.E.H. and F.L. designed and carried out all the electrochemical experiments. A.O. fabricated nanoparticle electrodes and carried out slim flow cell measurement. S.Z. and A.O. assisted with electrochemical experiments. A.S.R. and S.L. performed pH simulation with the assistance of Y.X. K.B. performed XPS measurements. A.O., F.L., F.P.G.d.A., M.L., X.W., Y.L., and D.S. contributed to data analysis and manuscript editing. J.E.H. and E.H.S. co-wrote the manuscript.

All authors discussed the results and assisted with the manuscript preparation. **Competing interests:** A provisional patent application US 63/200,393 titled "CO_2 electroreduction to multi-carbon products in strong acid" was filed on 4 March 2021 by the University of Toronto in the joint names of Total SE and the Governing Council of the University of Toronto. **Data and materials availability:** All experimental data are available in the main text or the supplementary materials.

SUPPLEMENTARY MATERIALS

science.sciencemag.org/content/372/6546/1074/suppl/DC1
Materials and Methods
Figs. S1 to S19
Tables S1 to S6
References (*38*–*45*)

20 January 2021; accepted 28 April 2021
10.1126/science.abg6582

Science

CO_2 electrolysis to multicarbon products in strong acid

Jianan Erick Huang, Fengwang Li, Adnan Ozden, Armin Sedighian Rasouli, F. Pelayo García de Arquer, Shijie Liu, Shuzhen Zhang, Mingchuan Luo, Xue Wang, Yanwei Lum, Yi Xu, Koen Bertens, Rui Kai Miao, Cao-Thang Dinh, David Sinton and Edward H. Sargent

Science **372** (6546), 1074-1078.
DOI: 10.1126/science.abg6582

Potassium helps CO_2 compete in acid

Electrochemical reduction of carbon dioxide (CO_2) is a promising means of converting this greenhouse gas into valuable fuels and chemicals. However, two competing reactions restrict the efficiency of this process. In base, much of the CO_2 is trapped as carbonate before reduction; in acid, protons outpace CO_2 at catching electrons from the cathode. Huang *et al.* report that a high dose of potassium ions can help to solve the latter problem. By concentrating potassium ions at the electrode, high selectivity toward CO_2 reduction at high current in acid is possible, which the authors attribute to electrostatic stabilization of the desired adsorbates.

Science, abg6582, this issue p. 1074

Science (print ISSN 0036-8075; online ISSN 1095-9203) is published by the American Association for the Advancement of Science, 1200 New York Avenue NW, Washington, DC 20005. The title *Science* is a registered trademark of AAAS.